Dynamic streaming potential coupling coefficient in porous media with different pore size distributions

Luong Duy Thanh, Damien Jougnot, Santiago Solazzi, van Nghia Nguyen, Phan Van do

submitted to *Geophys. J. Int.*

Dynamic streaming potential coupling coefficient in porous media with different pore size distributions

Luong Duy Thanh[1*], Damien Jougnot[2], Santiago G. Solazzi [3], Nguyen Van Nghia [1] and Phan Van Do [1]

[1] *Thuyloi University, 175 Tay Son, Dong Da, Ha Noi, Vietnam*

[2] *Sorbonne Université, CNRS, EPHE, UMR 7619 Metis, F-75005, Paris, France*

[3] *University of Lausanne, Institute of Earth Sciences, Lausanne, Switzerland*

[*] *Email: thanh_lud@tlu.edu.vn*

SUMMARY

Seismoelectric signals are generated by electrokinetic coupling from seismic wave propagation in fluid-filled porous media. This process is directly related to the existence of an electrical double layer at the interface between the pore fluid and minerals composing the pore walls. The seismoelectric method attracts the interest of researchers in different areas, from oil and gas reservoir characterization to hydrogeophysics, due to the sensitivity of the seismoelectric signals to medium and fluid properties. In this work, we propose a physically-based model for the dynamic streaming potential coupling coefficient (SPCC) by conceptualizing a porous medium as a bundle of tortuous capillaries characterized by presenting different pore size distributions (PSD). The results show that the dynamic streaming potential coupling coefficient is a complex function depending on the properties of pore fluid, mineral-pore fluid interfaces, microstructural parameters of porous media and frequency. Parameters influencing the dynamic SPCC are investigated and explained. In particular, we show that the PSD affects the transition frequency as well as

the shape of the SPCC response as a function of frequency. The proposed model is then compared with published data and previous models. It is found that the approach using the lognormal distribution is in very good agreement with experimental data as well as with previous models. Conversely, the approach that uses the fractal distribution provides a good match with published data for sandstone samples but not for sand samples. This result implies that the fractal PSD may not be pertinent for the considered sand samples, which exhibit a relatively narrow distribution of pore sizes. Our proposed approach can work for any PSD, for example, including complex ones such as double porosity or inferred from direct measurements. This makes the proposed models more versatile than models available in literature.

Keywords: Numerical modelling; Fractals and multifractals; Permeability and porosity

List of Symbols

Symbols	Description	Units
A	Normalizing factor	no units
$C_{EK}(r,\omega)$	Dynamic streaming potential coupling coefficient for a capillary of radius r	V/Pa
C_{EK}^{0}	Quasi-static streaming potential coupling coefficient	V/Pa
$C_{EK}(\omega)$	Dynamic streaming potential coupling coefficient	V/Pa
$C_{EK}^{rel}(\omega)$	Relative dynamic streaming potential coupling coefficient	no units
C^{w}	Ionic concentration	mol/L
D_f	Fractal dimension for pore space	no units
L_o	Length of the representative elementary volume (REV)	m
L_τ	Length of the capillary	m
r	Capillary radius	m
r_m	Geometric mean pore radius	m
r_{min}	Minimum capillary radius	m
r_{max}	Maximum capillary radius	m
α	Ratio between r_{min} and r_{max}	no units
ΔP^*	Amplitude of pressure difference	Pa
ϵ	Permittivity of the pore water	F/m
ϵ_0	Permittivity of vacuum (8.86×10^{-12})	F/m
ϵ_r	Relative permittivity of water (80.1)	no units
ζ	Zeta potential	V
η_w	Water viscosity ($\approx 10^{-3}$)	Pa s
ρ_w	Water density (≈ 1000)	kg/m^3
s	Lognormal standard deviation	no units
σ_w	Electrical conductivity of pore water	S/m
Σ_s	Surface electrical conductance	S
ω	Angular frequency	rad/s
ω_t	Transition angular frequency	rad/s

1 INTRODUCTION

Seismoelectric signals are generated by electrokinetic coupling from seismic wave propagation in fluid-filled porous media and are directly related to the existence of an electrical double layer (EDL)

at the interface between pore fluid and mineral surfaces. Minerals composing geological media generally acquire electrostatic charges at their surfaces when brought into contact with an electrolyte, such as water. This leads to a charge distribution known as the EDL prevailing at the vicinity of the water-mineral solid interfaces. The EDL consists of an excess of electrical charges in the pore water to compensate for the charged mineral surfaces. When a seismic wave propagates in fluid-filled porous media, it generates relative displacement of water with respect to the pore walls and, thus, relative movement of the charges in the EDL with respect to the charged pore surface. This process creates an electrical current and a resulting electrical field that can be measured at the earth surface or within a geological medium. Given the sensitivity of the seismoelectric signal to medium and fluid properties, the seismoelectric method attracts the interest of researchers in different areas, from oil and gas reservoir characterization to hydrogeophysics (e.g., Butler 1996; Mikhailov et al. 2000; Garambois & Dietrich 2001; Thompson et al. 2007). Additionally, it is indicated that the seismoelectric method is also feasible in well logging for oil and gas exploration (e.g., Dupuis et al. 2009; Hu et al. 2007; Wang et al. 2015a).

The seismoelectrical effect was studied by pioneering authors in the 1930′s (e.g., Thompson 1939; Frenkel 1944) and it remains a highly active research field (e.g., Pride & Garambois 2005; Revil et al. 2015; Jouniaux & Zyserman 2016; Jougnot & Solazzi 2021). To model the seismoelectric effect, one normally uses the electrokinetic coupling coefficient $C_{EK}(\omega)$, which is a frequency dependent parameter that relates the measured electrical potential difference with the fluid pressure difference driving the pore fluid flow. Several models have been proposed to describe $C_{EK}(\omega)$ in the literature. The two most used models for $C_{EK}(\omega)$ were proposed by (i) Packard (1953) and (ii) Pride (1994). Packard (1953) proposed a model for $C_{EK}(\omega)$ that is valid for capillary tubes. Pride (1994) obtained $C_{EK}(\omega)$ based on first principles and an upscaling approach based on volume averaging. Both of these models provide a good agreement with respect to measured data of the frequency dependent streaming potential (e.g., Reppert et al. 2001; Tardif et al. 2011; Glover et al. 2012a; Jouniaux & Ishido 2012; Wang et al. 2015b, 2016) and the seismoelectric conversion (Zhu et al. 1999; Zhu & Toksoz 2013). Note that the dependence of $C_{EK}(\omega)$ on thickness of the EDL was also presented by Shi et al. (2018).

An alternative approach was proposed for the determination of the streaming potential coupling coefficient via the excess charge that is effectively dragged by the flow of pore water through the pore space (e.g., Kormiltsev et al. 1998; Revil & Leroy 2004; Revil et al. 2007; Jougnot et al. 2012, 2020). A similar approach was proposed for the seismoelectric effect using effective excess charge density (e.g., Revil & Jardani 2010). The effective excess charge density can be determined either by an empirical expression from permeability of porous media (e.g., Jardani et al. 2007; Revil & Jardani 2013; Cherubini et al. 2018) or by a theoretical expression from macroscopic hydraulic parameters

and electrokinetic parameters of porous media (e.g., Guarracino & Jougnot 2018; Soldi et al. 2019). Revil & Mahardika (2013) proposed an empirical expression for the dependence of the effective excess charge density on frequency by taking into account a relaxation time governing the transition between the lowfrequency and highfrequency regimes of the Navier-Stokes equations. Very recently, Jougnot & Solazzi (2021) presented a novel approach to up-scale the frequency-dependent effective excess charge density from the pore scale by conceptualizing porous media as a bundle of capillaries having a singular capillary size.

It is well known that porous media usually have complicated and disordered pore structure with variation of pore sizes. Therefore, conceptualizing a porous medium as a bundle of capillaries with a unique pore size, as performed in Packard (1953) and Jougnot & Solazzi (2021), does not reflect the highly complex microstructure of porous media. Additionally, to the best of our knowledge, the surface electrical conductivity, a parameter that plays an important role in electrokinetics for low fluid electrical conductivity, has not yet been considered in the available models for $C_{EK}(\omega)$. Note that the surface electrical conductivity is typically taken into account in the streaming potential coupling coefficient, that is, the quasistatic coefficient via the modified Helmholtz-Smoluchowski equation (e.g., Morgan et al. 1989; Revil et al. 1999; Glover et al. 2012b).

Capillary tube models assume that flow channels are generated within the pore space. The characteristics of these channels are effectively represented employing the capillary tube geometry, using different tortuosities and pore radii distributions. Models based on this approach have, despite their simplicity, proven to be a highly effective tool for the realistic description of, for example, the water content (e.g., Tyler & Wheatcraft 1990), the permeability (e.g., Yu & Cheng 2002; Nghia A et al. 2021), the electrical conductivity (e.g., Niu et al. 2015; Thanh et al. 2019; Rembert et al. 2020), the thermal conductivity (e.g., Chu et al. 2020), the electrokinetic coupling (e.g., Jackson 2010; Soldi et al. 2019; Vinogradov et al. 2021) and the water flow in frozen soils (e.g., Watanabe & Flury 2008).

This work proposes a physically-based model for the $C_{EK}(\omega)$ by conceptualizing porous media as a bundle of tortuous capillaries. We consider both lognormal and fractal pore size distributions. We also analyze the effects of the surface electrical conductivity in the proposed model. Parameters influencing $C_{EK}(\omega)$ are investigated and explained. The proposed model is then compared with published data and previous models.

2 THEORETICAL DEVELOPMENT

2.1 Pore scale

Let us consider a capillary of radius r (m) and length L_τ (m) that is saturated by water with viscosity $\eta_w = 10^{-3}$ (Pa s) and density $\rho_w = 1000$ (kg/m^3) at temperature 20^{o}C. This capillary is submitted to an oscillatory frequency-dependent pressure difference ΔP (Pa) of angular frequency ω (rad/s) which is given by

$$\Delta P(t) = \Delta P^* e^{-i\omega t}, \tag{1}$$

where t (s) is the time, ΔP^* (Pa) is the amplitude of pressure difference across the capillary tube and i is the imaginary unit. The superscript * denotes the amplitude of the oscillatory pressure difference and of other oscillatory variables from now on. Following previous publications (e.g., Reppert et al. 2001; Solazzi et al. 2020; Jougnot & Solazzi 2021), we drop the harmonic term $e^{-i\omega t}$ to simplify the notation.

From the Navier-Stokes equations, it is possible to obtain the water velocity profile in the capillary as a function of the distance from the axis of the capillary x and the angular frequency $v^*(x,\omega)$ (m/s) (e.g., Packard 1953; Reppert et al. 2001). Additionally, the distribution of the excess charges $\rho_e(x)$ (C/m^3) in the pore water can be attained by solving the Poisson-Boltzmann equation (e.g., Rice & Whitehead 1965). From $v^*(x,\omega)$ and $\rho_e(x)$, one can find the streaming current in the capillary using the approach that has been already presented by Packard (1953) or Reppert et al. (2001). Using the assumptions of Debye-Hückel and a thin EDL (i.e., the thickness of the double layer is small compared to the pore radius), the frequency dependent streaming current $i_c(r,\omega)$ in the capillary of radius r (m) under the pressure difference ΔP^* is given by (e.g., Packard 1953; Reppert et al. 2001)

$$i_c^*(r,\omega) = \frac{2\pi\epsilon r\zeta\Delta P^*(\omega)}{\eta_w L_\tau \kappa}\frac{J_1(\kappa r)}{J_0(\kappa r)}, \tag{2}$$

where $\epsilon = \epsilon_r\epsilon_0$ (F/m) is the permittivity of the pore water with the permittivity of vacuum $\epsilon_0 = 8.86\times10^{-12}$ F/m and the relative permittivity of water ϵ_r=80.1 at temperature 20^{o}C, ζ (V) is the zeta potential, J_0 and J_1 are the first kind Bessel functions of the zeroth and first order, respectively, and κ (m^{-1}) is defined as

$$\kappa^2 = -\frac{i\omega\rho_w}{\eta_w}. \tag{3}$$

In this work, we consider the thin EDL assumption, which is satisfied in a wide variety of natural systems (e.g., seawater) (see the discussion section in Jougnot et al. 2019). However, it is important to remark that that this assumption may fail when: (i) the pore fluid has a low salinity, such as porous sediments containing fresh water; (ii) the EDL thickness becomes comparable to the characteristic pore size, such is the case of clay rocks. In this context, the thick EDL assumption should be used

instead. For further details regarding the thin/thick EDL assumptions, we refer the readers to the work of Jackson & Leinov (2012).

The dependence of ζ (V) on the ionic concentration C^w (mol/L) of pore water is given by (e.g., Pride & Morgan 1991):

$$\zeta = \{a + b\log_{10}(C^w)\} \times 10^{-3}, \tag{4}$$

where a and b are fitting parameters. In this work, we use a = -6.43 mV and b = 20.85 mV reported by Jaafar et al. (2009) for silica-based rocks for modeling.

As a consequence of the streaming current in the capillary, an oscillatory electrical potential difference called the frequency dependent streaming potential $\Delta V^*(\omega)$ is built up between the ends of the capillary. This streaming potential causes a frequency dependent electric conduction current in the capillary, which, in turn, can be determined using Ohm′s law. By considering both bulk and surface electrical conductions in the water saturated capillary, the conduction current is given by (Birdi 2008; Thanh et al. 2018, 2020a)

$$i_c^*(r,\omega) = \frac{\Delta V^*(\omega)\sigma_w \pi r^2}{L_\tau} + \frac{\Delta V^*(\omega)\Sigma_s 2\pi r}{L_\tau} = \frac{\pi \Delta V^*(\omega)}{L_\tau}\left[\sigma_w r^2 + 2\Sigma_s r\right], \tag{5}$$

where σ_w is the electrical conductivity of the fluid and Σ_s is the specific surface conductance at the interface between fluid and the solid. Note that, following previous publications (e.g., Packard 1953; Reppert et al. 2001; Jougnot et al. 2013; Jougnot & Solazzi 2021), we do not take into account the frequency dependence of the electrical conductivity.

As performed in the DC case (Packard 1953; Reppert et al. 2001; Thanh et al. 2018, 2020a), at equilibrium, the streaming current is balanced by the conduction current in the capillary. Setting Eq. (2) equal to Eq. (5) and using the definition of $C_{EK}^*(r,\omega)$ as

$$C_{EK}^*(r,\omega) = \frac{\Delta V^*(\omega)}{\Delta P^*(\omega)}, \tag{6}$$

the following expression is obtained for a single capillary

$$C_{EK}^*(r,\omega) = \frac{\Delta V^*(\omega)}{\Delta P^*(\omega)} = \frac{\epsilon\zeta}{\eta_w(\sigma_w + \frac{2\Sigma_s}{r})}\frac{2}{\kappa r}\frac{J_1(\kappa r)}{J_0(\kappa r)}. \tag{7}$$

If the surface conductivity is negligible (Σ_s=0), Eq. (7) reduces to the model proposed by Packard (1953) or Reppert et al. (2001).

$$C_{EK}^*(r,\omega) = \frac{\Delta V^*(\omega)}{\Delta P^*(\omega)} = \frac{\epsilon\zeta}{\eta_w\sigma_w}\frac{2}{\kappa r}\frac{J_1(\kappa r)}{J_0(\kappa r)}. \tag{8}$$

2.2 REV scale

In order to obtain the upscaled electrical streaming current and conduction, we consider a cubic representative elementary volume (REV) of the porous media of side-length L_o and cross-section area

A_{REV}, the latter being perpendicular to the flow direction. In the presence of a fluid pressure gradient, flow channels are generated within the pore space. The characteristics of these channels are usually modelled employing the capillary tube analogy. In this context, the REV is conceptualized as composed by an equivalent bundle of capillary tubes with radii varying from a minimum pore radius r_{min} to a maximum pore radius r_{max}. The pore size distribution $f(r)$ in the REV is such that the number of capillary tubes with radius in the range from r to $r + \mathrm{d}r$ is given by $f(r)\mathrm{d}r$. Note that the pore size distributions $f(r)$ can be obtained from the hydrodynamic characteristic curves of a porous medium, using either the capillary pressure-saturation or relative permeability-saturation relationships (e.g., Jougnot et al. 2012).

Following the approach used in Thanh et al. (2018) for the DC case, the frequency dependent streaming current $I_s^*(\omega)$ and conduction current $I_c^*(\omega)$ through the REV are given by

$$I_s^*(\omega) = \int_{r_{min}}^{r_{max}} i_s^*(r,\omega) f(r) dr = \int_{r_{min}}^{r_{max}} \frac{2\pi\epsilon r \zeta \Delta P^*(\omega)}{\eta_w L_\tau \kappa} \frac{J_1(\kappa r)}{J_0(\kappa r)} f(r) dr, \tag{9}$$

and

$$I_c^*(\omega) = \int_{r_{min}}^{r_{max}} i_c^*(r,\omega) f(r) dr = \int_{r_{min}}^{r_{max}} \frac{\pi \Delta V^*(\omega)}{L_\tau} \left[\sigma_w r^2 + 2\Sigma_s r\right] f(r) dr. \tag{10}$$

We apply the similar procedure to get the $C_{EK}^*(r,\omega)$ at pore scale, that is, we set Eq. (9) equal to Eq. (10) and, then, we obtain the following expression for $C_{EK}^*(\omega)$ at the macro-scale:

$$C_{EK}^*(\omega) = \frac{\int_{r_{min}}^{r_{max}} \frac{2\epsilon\zeta}{\eta_w \kappa} \frac{J_1(\kappa r)}{J_0(\kappa r)} r f(r) dr}{\int_{r_{min}}^{r_{max}} \left[\sigma_w r^2 + 2\Sigma_s r\right] f(r) dr}. \tag{11}$$

Recall that the transition from viscous to inertia dominated flow occurs at the so-called transition angular frequency ω_t above which the amplitude of fluid flow decreases with frequency, which is given by (e.g., Solazzi et al. 2020)

$$\omega_t = \frac{2\eta_w}{\rho_w \widetilde{r}^2}, \tag{12}$$

where $\widetilde{r}$ is a characteristic radius representative of the saturated pores.

In this work, we analyze two different PSDs: (i) lognormal and (ii) fractal distributions, for modeling $C_{EK}^*(\omega)$ as presented below. However, it is important to remark that Eq. (11) has been built up for any pore size distribution $f(r)$.

2.2.1 Lognormal Distribution

The lognormal distribution of capillary tubes is frequently applied to porous media (e.g., Kosugi 1994; Jougnot et al. 2019; Ghanbarian 2020) and is given by

$$f(r) = \frac{A}{\sqrt{2\pi}s\,r}\exp\left[-\left(\frac{\ln(\frac{r}{r_m})}{\sqrt{2}s}\right)^2\right], r_{min} \leq r \leq r_{max} \tag{13}$$

where A is a normalizing prefactor, r_m is the geometric mean pore radius, and s is the log-normal standard deviation. Note that the total number of capillaries N_t following the lognormal distribution in the REV is given by

$$N_t = \int_{r_{min}}^{r_{max}} f(r)dr = \frac{A}{2}\left\{\text{erf}\left(\frac{\ln(\frac{r_{max}}{r_m})}{\sqrt{2}s}\right) - \text{erf}\left(\frac{\ln(\frac{r_{min}}{r_m})}{\sqrt{2}s}\right)\right\} \tag{14}$$

Similarly, substituting Eq. (13) into Eq. (11), we obtain the $C^*_{EK}(\omega)$ with the lognormal distribution as:

$$C^{log,*}_{EK}(\omega) = \frac{\epsilon\zeta}{\eta}\frac{\int_{r_{min}}^{r_{max}}\left\{\frac{2}{\kappa r}\frac{J_1(\kappa r)}{J_0(\kappa r)}r\exp\left[-\left(\frac{\ln(\frac{r}{r_m})}{\sqrt{2}s}\right)^2\right]\right\}dr}{\sigma_w\int_{r_{min}}^{r_{max}} r\exp\left[-\left(\frac{\ln(\frac{r}{r_m})}{\sqrt{2}s}\right)^2\right]dr + 2\Sigma_s\int_{r_{min}}^{r_{max}}\exp\left[-\left(\frac{\ln(\frac{r}{r_m})}{\sqrt{2}s}\right)^2\right]dr}. \tag{15}$$

For sufficiently low frequencies, Eq. (15) reduces to

$$C^{log,0}_{EK} = \frac{\epsilon\zeta}{\eta}\frac{\int_{r_{min}}^{r_{max}} r\exp\left[-\left(\frac{\ln(\frac{r}{r_m})}{\sqrt{2}s}\right)^2\right]dr}{\sigma_w\int_{r_{min}}^{r_{max}} r\exp\left[-\left(\frac{\ln(\frac{r}{r_m})}{\sqrt{2}s}\right)^2\right]dr + 2\Sigma_s\int_{r_{min}}^{r_{max}}\exp\left[-\left(\frac{\ln(\frac{r}{r_m})}{\sqrt{2}s}\right)^2\right]dr}, \tag{16}$$

where

$$\int_{r_{min}}^{r_{max}} r\exp\left[-\left(\frac{\ln(\frac{r}{r_m})}{\sqrt{2}s}\right)^2\right]dr = -\frac{\sqrt{\pi}}{\sqrt{2}}sr_m^2e^{2s^2}\left\{\text{erf}\left(\frac{2s^2-\ln(\frac{r_{max}}{r_m})}{\sqrt{2}s}\right) - \text{erf}\left(\frac{2s^2-\ln(\frac{r_{min}}{r_m})}{\sqrt{2}s}\right)\right\}, \tag{17}$$

and

$$\int_{r_{min}}^{r_{max}}\exp\left[-\left(\frac{\ln(\frac{r}{r_m})}{\sqrt{2}s}\right)^2\right]dr = -\frac{\sqrt{\pi}}{\sqrt{2}}sr_me^{\frac{s^2}{2}}\left\{\text{erf}\left(\frac{s^2-\ln(\frac{r_{max}}{r_m})}{\sqrt{2}s}\right) - \text{erf}\left(\frac{s^2-\ln(\frac{r_{min}}{r_m})}{\sqrt{2}s}\right)\right\}. \tag{18}$$

Substituting Eq. (17) and Eq. (18) into Eq. (16), the following is obtained

$$C^{log,0}_{EK} = \frac{\epsilon\zeta}{\eta}\frac{1}{\left[\sigma_w + \frac{2\Sigma_s e^{\frac{-3s^2}{2}}}{r_m}\frac{\left\{\text{erf}\left(\frac{s^2-\ln(\frac{r_{max}}{r_m})}{\sqrt{2}s}\right)-\text{erf}\left(\frac{s^2-\ln(\frac{r_{min}}{r_m})}{\sqrt{2}s}\right)\right\}}{\left\{\text{erf}\left(\frac{2s^2-\ln(\frac{r_{max}}{r_m})}{\sqrt{2}s}\right)-\text{erf}\left(\frac{2s^2-\ln(\frac{r_{min}}{r_m})}{\sqrt{2}s}\right)\right\}}\right]} \tag{19}$$

Following Jougnot & Solazzi (2021), we can write Eq. (15) as

$$C^{log,*}_{EK}(\omega) = C^{log,0}_{EK}C^{rel,log,*}_{EK}(\omega), \tag{20}$$

where $C_{EK}^{rel,log,*}(\omega)$ is the frequency dependent relative streaming potential coefficient for the lognormal distribution with respect to the value at 0 Hz and is given by

$$C_{EK}^{rel,log,*}(\omega) = \frac{\int_{r_{min}}^{r_{max}} \left\{ \frac{2}{\kappa r} \frac{J_1(\kappa r)}{J_0(\kappa r)} r \exp\left[-\left(\frac{\ln(\frac{r}{r_m})}{\sqrt{2}s} \right)^2 \right] \right\} dr}{\int_{r_{min}}^{r_{max}} r \exp\left[-\left(\frac{\ln(\frac{r}{r_m})}{\sqrt{2}s} \right)^2 \right]}. \tag{21}$$

2.2.2 Fractal Distribution

Fractal distribution has been already applied for porous media in many publications (e.g., Yu & Cheng 2002; Guarracino & Jougnot 2018; Soldi et al. 2019; Thanh et al. 2020b,c). The fractal distribution of capillary tubes is given by (e.g., Tyler & Wheatcraft 1990; Yu & Cheng 2002; Thanh et al. 2020b)

$$f(r) = D_f r_{max}^{D_f} r^{-D_f - 1}, \tag{22}$$

where D_f is the fractal dimension for pore space that is between 1 and 2 in two-dimensional spaces and between 2 and 3 in three dimensional spaces. Note that the total number of capillaries N_t following the fractal distribution in the REV is given by

$$N_t = \int_{r_{min}}^{r_{max}} f(r) dr = \left(\frac{r_{max}}{r_{min}} \right)^{D_f} - 1 \approx \left(\frac{r_{max}}{r_{min}} \right)^{D_f}. \tag{23}$$

Here, we consider that $r_{max} >> r_{min}$, that is, $\left(\frac{r_{max}}{r_{min}} \right)^{D_f}$ is much larger than 1, which is normally valid in porous media (e.g., Yu & Cheng 2002; Thanh et al. 2020b).

Substituting Eq. (22) into Eq. (11), we obtain the $C_{EK}^{*}(\omega)$ with the fractal distribution as:

$$C_{EK}^{fra,*}(\omega) = \frac{\epsilon \zeta}{\eta \left[\sigma_w + \frac{2\Sigma_s}{r_{max}} \frac{2-D_f}{1-D_f} \frac{1-\alpha^{1-D_f}}{1-\alpha^{2-D_f}} \right]} \frac{2-D_f}{(1-\alpha^{2-D_f}) r_{max}^{2-D_f}} \int_{r_{min}}^{r_{max}} \frac{2}{\kappa r} \frac{J_1(\kappa r)}{J_0(\kappa r)} r^{1-D_f} dr, \tag{24}$$

where $\alpha = r_{min}/r_{max}$.

Eq. (15) and Eq. (24) indicate that the dynamic streaming potential coupling coefficient is a complex function depending on the properties of water (η, σ_w, ϵ), mineral-water interfaces (ζ, Σ_s), microstructural parameters of porous media (D_f, r_{min}, r_{max} for the fractal distribution and r_m, s, r_{min}, r_{max} for the lognormal distribution) and frequency (ω).

When $\omega \to 0$, the pressure difference tends to a steady-state condition across the REV and, thus, the parameter κ approaches zero as indicated by Eq. (3). The limit of $\left\{ \frac{2}{\kappa r} \frac{J_1(\kappa r)}{J_0(\kappa r)} \right\}$ becomes (e.g., Packard 1953; Reppert et al. 2001)

$$\lim_{\kappa \to 0} \left\{ \frac{2}{\kappa r} \frac{J_1(\kappa r)}{J_0(\kappa r)} \right\} = 1. \tag{25}$$

Therefore, the integral term in Eq. (24) reduces to

$$\lim_{\kappa\to 0}\left\{\int_{r_{min}}^{r_{max}} \frac{2}{\kappa r}\frac{J_1(\kappa r)}{J_0(\kappa r)} r^{1-D_f} dr\right\} = \frac{r_{max}^{2-D_f}}{2-D_f}(1-\alpha^{2-D_f}), \tag{26}$$

and Eq. (24) becomes

$$C_{EK}^{fra,0} = \frac{\epsilon\zeta}{\eta\left[\sigma_w + \frac{2\Sigma_s}{r_{max}}\frac{2-D_f}{1-D_f}\frac{1-\alpha^{1-D_f}}{1-\alpha^{2-D_f}}\right]}. \tag{27}$$

Note that, in Eq. (27), the proposed model reduces to that of Thanh et al. (2018), which was proposed and validated for DC conditions.

If the surface conductivity can be neglected (Σ_s = 0), Eq. (19) and Eq. (27) reduce to the widely used Helmholtz-Smoluchowski (HS) equation which does not include information about the medium geometrical properties and has been proven to be useful in a large range of natural geological media Smoluchowski (1903). Namely, the HS equation is given by

$$C_{EK}^{HS} = \frac{\epsilon\zeta}{\eta\sigma_w}. \tag{28}$$

It is also shown that the PSD does not have effect on the quasi-static streaming potential coupling coefficient as long as the surface conductivity is negligible, which is in agreement with the result reported in Jougnot et al. (2019).

Similarly, the frequency dependent relative streaming potential coupling coefficient for the fractal PSD with respect to the zero frequency is given by

$$C_{EK}^{rel,fra,*}(\omega) = \frac{2-D_f}{(1-\alpha^{2-D_f})r_{max}^{2-D_f}}\int_{r_{min}}^{r_{max}} \frac{2}{\kappa r}\frac{J_1(\kappa r)}{J_0(\kappa r)} r^{1-D_f} dr. \tag{29}$$

Eq. (29) can be solved numerically once the parameters D_f, r_{min} and r_{max} of porous media are defined.

3 RESULTS AND DISCUSSION

3.1 Sensitivity of the model

3.1.1 Dynamic streaming potential coupling coefficient in a single capillary

Figure 1 shows the dynamic relative streaming potential coupling coefficient $C_{EK}^{*}(r,\omega)$ as a function of frequency for a single capillary predicted Eq. (7): (a) real component and (b) imaginary component of $C_{EK}^{*}(r,\omega)$. In Eq. (7), we use representative values of r = 10 μm, $C^w = 10^{-3}$ mol/L (from Eq. (4), ζ is obtained) and three representative values Σ_s (0, 5×10^{-9} and 10×10^{-9} S). Note that we consider $C^w = 10^{-3}$ mol/L as it has been proven to be a pertinent value in the context of groundwater studies (e.g., Jackson et al. 2012). The range of Σ_s between 0 and 10×10^{-9} S is commonly reported for

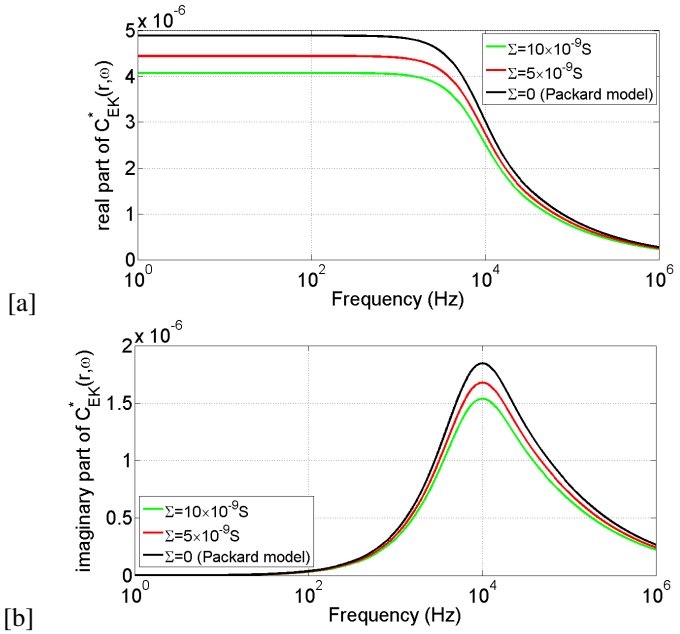

Figure 1. Dynamic relative streaming potential coupling coefficient $C^*_{EK}(r,\omega)$ as a function of frequency for a single capillary predicted Eq. (7) for representative values of r = 10 μm, C^w = 10^{-3} mol/L (from Eq. (4), ζ is obtained) and three values Σ_s (0, 5×10^{-9} and 10×10^{-9}S): (a) real component and (b) imaginary component of $C^*_{EK}(r,\omega)$.

silica-based samples saturated by water (e.g., Revil & Glover 1998; Glover & Dery 2010). The case with $\Sigma_s = 0$ S corresponds to the hypothesis of the model from Packard (1953). It is seen that the surface conductivity has an influence on real and imaginary part of $C^*_{EK}(r,\omega)$. When ignoring the surface conductivity, one may overestimate the $C^*_{EK}(r,\omega)$, especially for small capillaries and low ionic concentration.

3.1.2 Quasi-static streaming potential coupling coefficient in porous media

As previously mentioned, we employ fractal and lognormal PSDs (see Figure 2) for pore sizes ranging from r_{min} = 1 μm to r_{max} = 100 μm. In particular, we consider the following characteristics for the PSD: (a) fractal with D_f = 1.4; (d) fractal with D_f = 1.8; (b) lognormal with r_m = r_{max}/3 and $s = 0.1$; (e) lognormal with r_m = r_{max}/20 and $s = 0.1$; (c) lognormal with r_m = r_{max}/3 and $s = 0.1$; (f) lognormal with r_m = r_{max}/3 and $s = 0.4$. Note that D_f, r_m, r_{min}, r_{max} and s can be selected with different values.

Figure 3 shows the variation of the quasi-static streaming potential coupling coefficient C^0_{EK} with ionic concentration. Fig. 3 (a) is predicted from Eq. (27) for the fractal distribution with three values of D_f (1.4, 1.6, 1.8). Fig. 3 (b), (c) are predicted Eq. (19) for the lognormal distribution with three values of r_m (r_{max}/3, r_{max}/10, r_{max}/20 while fixing s = 0.1) and three values of s (0.1, 0.25, 04 while

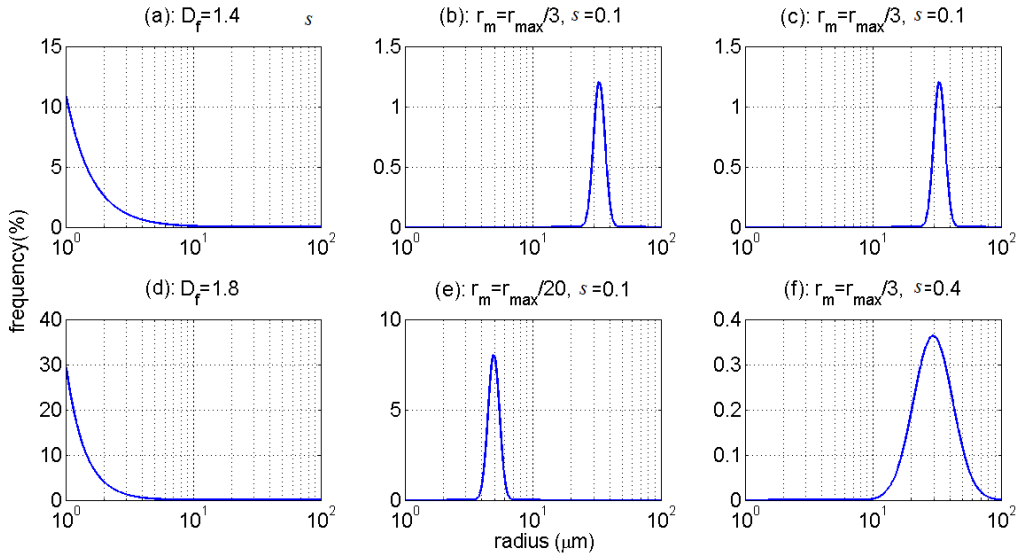

Figure 2. PSDs used in this work. We consider r_{min} = 1 μm and r_{max} = 100 μm, and illustrate: (a) fractal PSD with D_f = 1.4; (d) fractal PSD with D_f = 1.8; (b) lognormal PSD with r_m = r_{max}/3 and $s = 0.1$; (e) lognormal PSD with r_m = r_{max}/20 and $s = 0.1$; (c) lognormal PSD with r_m = r_{max}/3, $s = 0.1$; (f) lognormal PSD with r_m = r_{max}/3 and $s = 0.4$.

fixing r_m = r_{max}/10), respectively. The surface conductance Σ_s is taken as 5×10^{-9} S. Fig. 3 (a) shows that the C^0_{EK} from the fractal distribution is sensitive to D_f and decreases with an increase of D_f at low ionic concentration C^w. When C^w is larger than a certain value, that means, the surface conductivity is negligible, C^0_{EK} approaches C^{HS}_{EK} (see black solid line) irrespective of the geometrical properties (D_f) of the medium. The reason for the decrease of C^0_{EK} with increasing D_f is that, when D_f increases, the number of capillaries characterized by relatively small radii increases, as shown by the shift from Fig. 2 (a) to (d). Consequently, the surface conductivity of the REV increases and, thus, C^0_{EK} decreases. Note that the surface conductivity of porous media is dominated by the contribution from the smaller capillaries for the same surface conductance and electrical conductivity of water. Fig. 3 (b) shows that the C^0_{EK} predicted from the lognormal distribution is sensitive to r_m and decreases with a decrease of r_m at low ionic concentration C^w. When C^w is larger than a certain value, C^0_{EK} approaches C^{HS}_{EK} irrespective of the r_m values, as discussed above (see black solid line). The decrease of C^0_{EK} with decreasing r_m is explained in the similar way to that of Fig. 3 (a). Namely, when r_m decreases, the number of smaller radius capillaries increases as shown by the shift from Fig. 2 (b) to (e). Consequently, the surface conductivity of the REV increases and C^0_{EK} decreases. Fig. 3 (c) shows that the C^0_{EK} is much less sensitive to the lognormal standard deviation s at low ionic concentration C^w. When C^w is larger than a certain value, C^0_{EK} also reduces to C^{HS}_{EK} (see black solid line). These results are consistent with previously published studies (e.g., Jougnot et al. 2019).

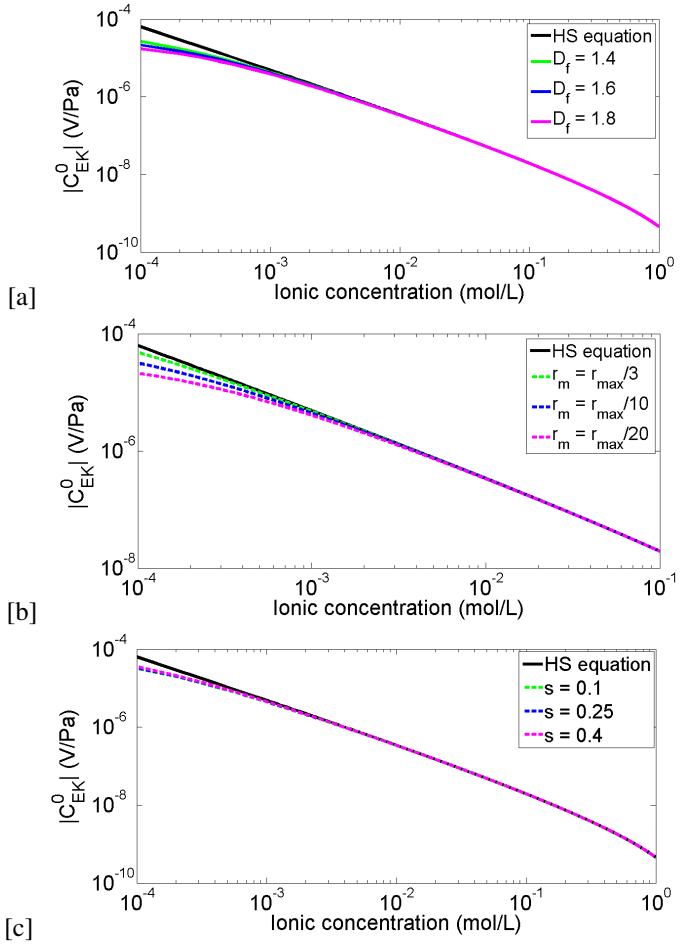

Figure 3. Variation of the quasi-static streaming potential coupling coefficient C^0_{EK} with ionic concentration: (a) is predicted from Eq. (27) for the fractal distribution with three values of D_f (1.4, 1.6, 1.8); (b), (c) are predicted from Eq. (19) for the lognormal distribution with three values of r_m (r_{max}/3, r_{max}/10, r_{max}/20 while fixing s = 0.1) and three values of s (0.1, 0.25, 04 while fixing r_m = r_{max}/10), respectively.

Recently, Vinogradov et al. (2021) proposed to use a rock-specific PSD directly extracted from the petrophysical characterization of a sample. This PSD is non-monotonic and follows a form given by three intervals:

$$f(r) = \begin{cases} B_1 \left(\frac{r-r_{min}}{r_{max}-r_{min}}\right)^{m_1}, & \text{for } r_{min} \leq r \leq r_1 \\ constant, & \text{for } r_1 < r < r_2 \\ B_2 \left(\frac{r-r_{max}}{r_{min}-r_{max}}\right)^{m_2}, & \text{for } r_2 < r \leq r_{max} \end{cases} \tag{30}$$

where B_1 and B_2 represent the normalisation factors of the first and third interval, respectively; $0 < m_1, m_2 < \infty$ (constant, unitless) are the respective skewing constants and r_1 and r_2 are limits of the second interval. The limits of each interval are determined by experimental data for the PSD. For example, for a sample of Berea sandstone reported in literature, Vinogradov et al. (2021) obtained r_{min}

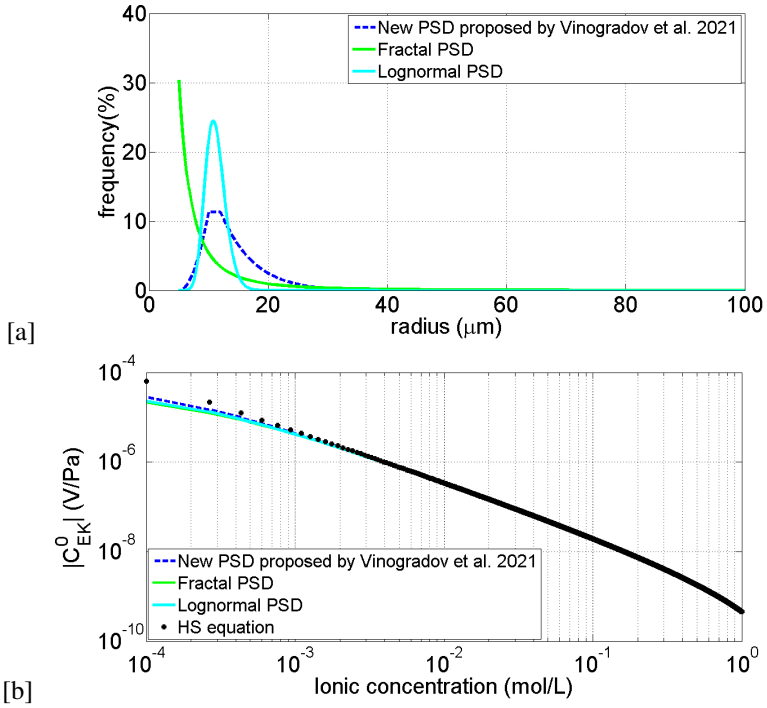

Figure 4. (a) A new PSD proposed by Vinogradov et al. (2021), fractal PSD (D_f = 1.5) and lognormal PSD (r_m = 11 μm and s = 0.15) in the same range of radii from r_{min} = 5 μm to r_{max} = 100 μm; (b) Variation of the quasi-static streaming potential coupling coefficient C^0_{EK} with ionic concentration for different PSDs (Σ_s = 5×10^{-9} S).

= 5 μm, r_{min} = 100 μm, B_1 = 119,990, B_2 = 1131, m_1 = 2 and m_2 = 16 and shown the corresponding PSD by the dashed line in Fig. 4 (a). The representative PSDs for fractal (D_f = 1.5) and lognormal (r_m = 11 μm and s = 0.15) in the same range of radii from r_{min} = 5 μm to r_{max} = 100 μm are also shown in Fig. 4 (a). With three different PSDs shown in Fig. 4 (a), we can predict the variation of C^0_{EK} with ionic concentration using the same approach as previously mentioned (see Fig. 4 (b) with $\Sigma_s = 5\times10^{-9}$ S). Note that we obtained C^0_{EK} numerically for a new PSD proposed by Vinogradov et al. (2021). The HS equation is also used for comparison in Fig. 4 (b). It is seen that the non-monotonic PSD proposed by Vinogradov et al. (2021) is quite relevant to the lognormal PSD that is later shown to be pertinent for both consolidated samples (e.g., rocks) or unconsolidated ones (e.g., sand packs). Therefore, the non-monotonic PSD proposed by Vinogradov et al. (2021) can provide realistic description of porous rocks and can be applied to study transport phenomena in porous media.

3.1.3 Dynamic streaming potential coupling coefficient in porous media

Figure 5 shows the dynamic relative streaming potential coupling coefficient as a function of frequency predicted from the lognormal distribution, given by Eq. (21) taking r_{min} = 1 μm, r_{max} = 100 μm, and

considering three representative values of r_m ($r_{max}/3$, $r_{max}/10$, $r_{max}/20$) and s = 0.1. We illustrate the (a) real component, (b) imaginary component and (c) phase of $C_{EK}^{rel,*}(\omega)$. For comparison, the black line represents Packard (1953) prediction given by Eq. (8) for a single capillary of radius r = 10 μm. It is observed that the general behavior of $C_{EK}^{rel,*}(\omega)$ predicted from Eq. (21) for porous media and that predicted from Eq. (8) for a single capillary are similar. The noticeable characteristic of the curves is that the transition frequency shifts to higher frequency when r_m decreases. This relationship is explained based on Eq. (12) for the transition frequency ω_t. Namely, when r_m decreases, the number of capillaries with smaller radii increases, as mentioned earlier. Consequently, the characteristic radius $\widetilde{r}$ decreases and the transition frequency ω_t increases with decreasing r_m. It is seen that the magnitude of the $C_{EK}^{rel,*}(\omega)$ is stable at low frequencies and decrease for frequencies greater than the transition frequency. The reason is that when the frequency increases, the inertia regime starts to prevail and the fluid movement starts to be increasingly out of phase with the applied oscillatory pressure, thus reducing the fluid velocity within the pore (e.g., Zhou & Sheng 1989). Therefore, the $C_{EK}^{rel,*}(\omega)$ decreases. Fig. 5 (a) and (b) shows that the real and imaginary parts of $C_{EK}^{rel,*}(\omega)$ follow the similar behaviors for different values of r_m and decrease at the same rate at high frequencies. This explains the 45^o phase angle found at high frequencies as shown in Fig. 5 (c) and that is in agreement with Reppert et al. (2001).

Figure 6 shows the dynamic relative streaming potential coupling coefficient as a function of frequency predicted from the lognormal distribution with r_{min} = 1 μm, r_{max} = 100 μm for three different values of s (0.1, 0.25, 0.4) and a representative of r_m = r_{max}/10: (a) real component and (b) imaginary component of $C_{EK}^{rel,*}(\omega)$. Again, the black solid line is predicted from Packard (1953) given by Eq. (8) for a single capillary of radius r = r_{max}/10 = 10 μm for comparison. We note that the observed behaviors in Fig. 6 are similar to Fig. 5. The coefficient $C_{EK}^{rel,*}(\omega)$ is sensitive to s and ω_t decreases with an increase of s for a given value of r_m. The reason is that when s increases, $\widetilde{r}$ increases (see shift from Fig. 2 (c) to (f)). Consequently, ω_t decreases with increasing s.

Figure 7 shows the dynamic relative streaming potential coupling coefficient as a function of frequency predicted from the fractal distribution, given by Eq. (29) taking r_{min} = 1 μm, r_{max} = 100 μm for three representative values of D_f (1.4, 1.6, 1.8): (a) real component and (b) imaginary component of $C_{EK}^{rel,*}(\omega)$. The black solid line is predicted from Packard (1953) given by Eq. (8) for a single capillary of radius r = 10 μm for comparison. It is observed that, regardless of D_f, the real component of the $C_{EK}^{rel,*}(\omega)$ is rather stable at low frequencies and decrease for frequencies greater than a given threshold value. It is seen that Eq. (29) can reproduce the main trend predicted by the model of Packard (1953) that is valid for a single capillary at low frequency. However, the behavior diverges for higher frequencies. We also observe that the transition frequency ω_t for porous media

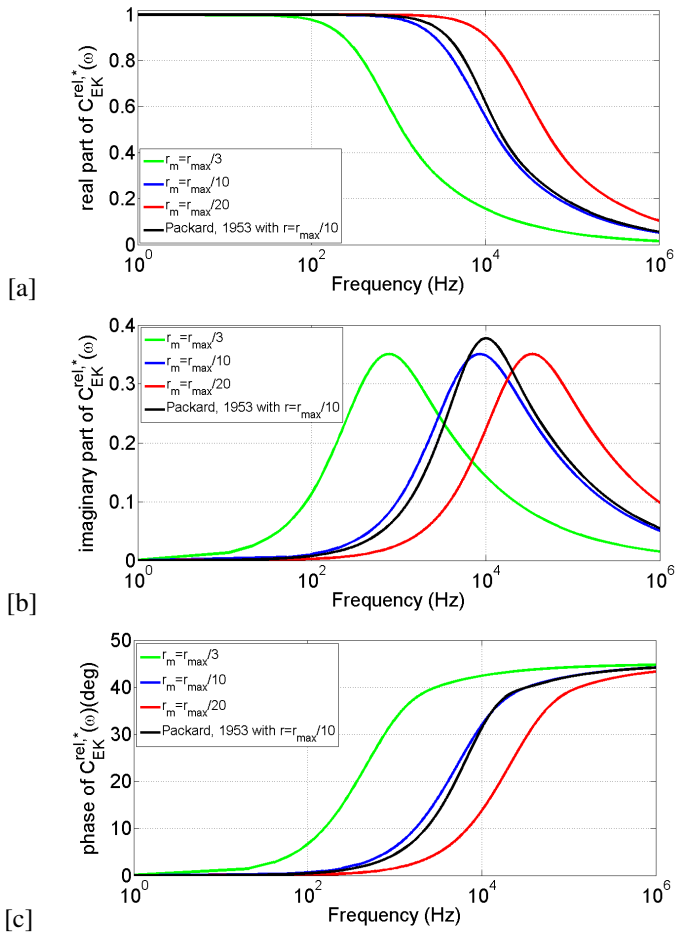

Figure 5. The dynamic relative streaming potential coupling coefficient as a function of frequency predicted from the lognormal distribution - Eq. (21) with r_{min} = 1 μm, r_{max} = 100 μm for three representative values of r_m ($r_{max}/3$, $r_{max}/10$, $r_{max}/20$) and a representative of s = 0.1: (a) real component, (b) imaginary component and (c) phase (in degree) of $C_{EK}^{rel,*}(\omega)$. The black line is predicted from Packard (1953) given by Eq. (8) for a single capillary of radius r = 10 μm for comparison.

moves to higher frequencies with an increase of D_f. The reason for this is that when D_f increases, the number of capillaries with small radius increases. Consequently, the characteristic radius $\widetilde{r}$ decreases and the transition frequency ω_t increases with increasing D_f.

3.1.4 Comparison with published data

Figure 8 shows the variation of the magnitude of $C_{EK}^{*}(\omega)$ as a function of frequency measured by Zhu & Toksoz (2013) for a Berea sandstone sample (permeability k = 450×10^{-15} m^2 and porosity ϕ = 0.23) saturated by different pore water conductivities. The proposed model with lognormal and fractal distributions is used to explain the experimental data (see solid lines in Fig. 8 (a) and (b), respectively). As reported by Zhu & Toksoz (2013), we consider the values of C_{EK}^{0} are 0.3×10^{-6},

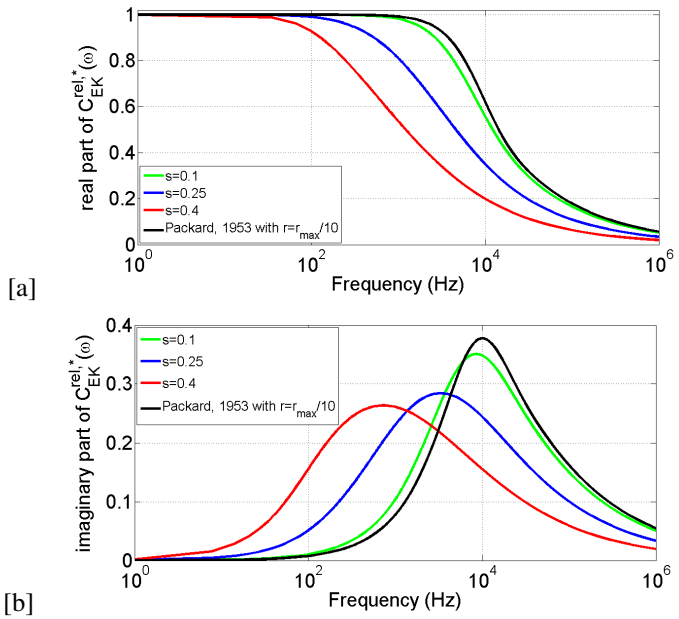

Figure 6. The dynamic relative streaming potential coupling coefficient as a function of frequency predicted from the lognormal distribution with r_{min} = 1 μm, r_{max} = 100 μm for three different values of s (0.1, 0.25, 0.4) and a representative of $r_m = r_{max}/10$: (a) real component and (b) imaginary component of $C_{EK}^{rel,*}(\omega)$. The black line is predicted from Packard (1953) given by Eq. (8) for a single capillary of radius $r = r_{max}/10$ for comparison.

0.15×10^{-6}, 0.065×10^{-6}, 0.035×10^{-6} and 0.024×10^{-6} V/Pa for 0.012, 0.048, 0.095, 0.18 and 0.32 S/m, respectively. From Eq. (21) and Eq. (29), we can obtain $C_{EK}^{rel,*}(\omega)$ with fitting parameters and therefore $C_{EK}^{*}(\omega)$. Note that, due to numerical constraints associated with the integrations indicated by Eq. (21) and Eq. (29), we do not intent here to perform an exhaustive inversion of the parameters of the proposed model from experimental datasets. Our intention is to show that the proposed approach is capable of reproducing experimental results and, thus, we empirically search for the parameters that provide a relatively good fit. For the lognormal PSD, we found that the parameters r_m = 5.8 μm, s = 0.1, r_{min} = 0.13 μm and r_{max} = 27 μm provide a good fit. For the fractal PSD, a good fit is obtained for D_f = 1.5, r_{min} = 0.13 μm and r_{max} = 27 μm. It is seen that the proposed model using both distributions predicts very well the experimental data. The root mean square deviation (RMSD) for the lognormal and fractal distributions are 1.15×10^{-9} and 2.23×10^{-9} V/Pa. Therefore, the lognormal distribution provides a slightly better result than the fractal distribution.

Figure 9 shows the variation of the magnitude of $C_{EK}^{rel,*}(\omega)$ as a function of frequency measured by Peng et al. (2020) for a sandstone sample with ϕ = 0.0390 and k = 10.1 mD. The proposed model with the lognormal and fractal distributions is also used to reproduce experimental data. For the lognormal PSD, the data is fitted by taking r_m = 1.4 μm, s = 0.1, r_{min} = 24 nm and r_{max} = 4.7 μm. For the

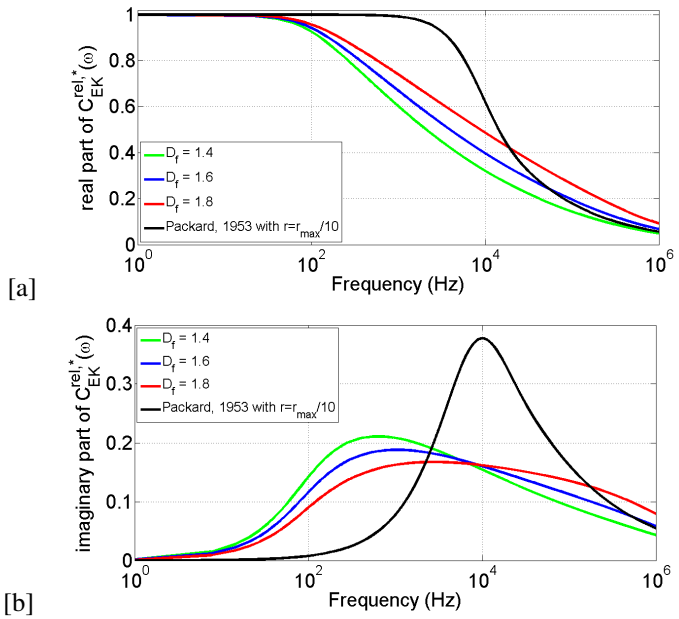

Figure 7. The dynamic relative streaming potential coupling coefficient as a function of frequency predicted from the fractal distribution - Eq. (29) for r_{min} = 1 μm, r_{max} = 100 μm and three values of D_f (1.4, 1.6, 1.8): (a) real component and (b) imaginary component of the $C_{EK}^{rel,*}(\omega)$. The black solid line is predicted from Packard (1953) given by Eq. (8) for a single capillary of radius r = r_{max}/10 for comparison.

fractal PSD, we take D_f = 1.6, r_{min} = 24 nm and r_{max} = 4.7 μm. We observe that the proposed model using the lognormal and fractal PSDs can reproduce experimental data reported by Peng et al. (2020). It seems that, in this case, the fractal PSD provides a slightly better prediction than the lognormal PSD (RMSD values for the lognormal and fractal PSDs are 0.022 and 0.003). At high frequency, as seen in Fig. 9 and later figure, the magnitude of $C_{EK}^{rel,*}$ for the lognormal PSD decreases with increasing frequency at a higher rate than that for the fractal PSD.

Note that r_{max} of porous media can be predicted from permeability using an expression suggested by Cai & Yu (2010)

$$r_{max} = \frac{1}{2}\sqrt{32\tau k\frac{(4-D_f)(1-\phi)}{(2-D_f)\phi}}, \tag{31}$$

where τ is the tortuousity of porous media which can be estimated using $\tau = \sqrt{1-2.02\ln(\phi)}$ given by Peng et al. (2020). From Eq. (31), r_{max} is estimated to be 15 μm and 5.7 μm for the samples reported by Zhu & Toksoz (2013) and Peng et al. (2020), respectively. Those values are reasonably good agreement with ones we obtained when fitting the data with our models (27 μm and 4.7 μm, respectively).

Figure 10 shows the variation of the magnitude of $C_{EK}^{rel,*}(\omega)$ as a function of frequency measured by Wang et al. (2015b) for a sandstone sample (ϕ = 0.302 and k = 1435 mD) with an error bar of

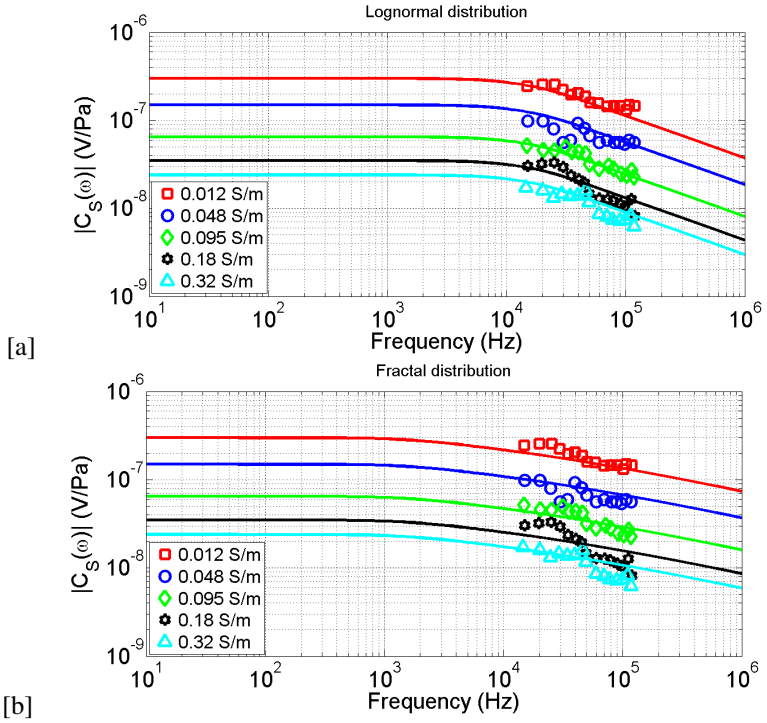

Figure 8. Comparison between the amplitude of C^*_{EK} as a function of frequency (symbols) measured by Zhu & Toksoz (2013) and the model predictions (solid lines): (a) lognormal PSD with the best parameters of r_m = 5.8 μm, s = 0.1, r_{min} = 0.13 μm and r_{max} = 27 μm; (b) fractal PSD with the fitting parameters of D_f = 1.5, r_{min} = 0.13 μm and r_{max} = 27 μm.

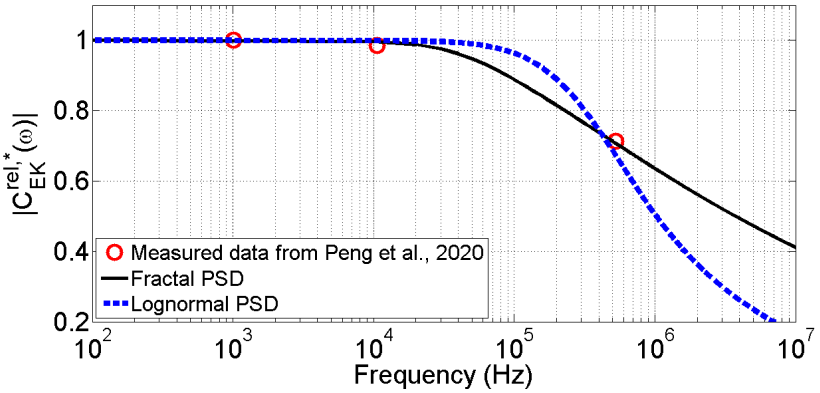

Figure 9. Comparison between the amplitude of $C^{rel,*}_{EK}$ as a function of frequency for a sandstone sample measured by Peng et al. (2020) and the model predictions: (a) lognormal PSD with fitting parameters of r_m = 1.4 μm, s = 0.1, r_{min} = 24 nm and r_{max} = 4.7 μm; (b) fractal PSD with fitting parameters of D_f = 1.6, r_{min} = 24 nm and r_{max} = 4.7 μm.

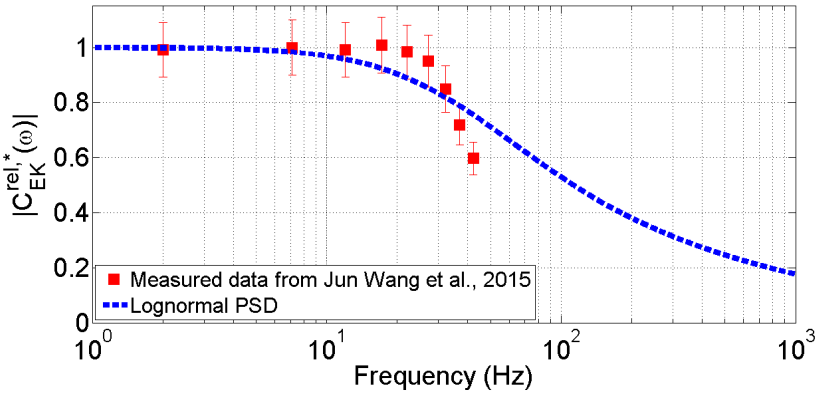

Figure 10. Comparison between the amplitude of $C_{EK}^{rel,*}$ as a function of frequency for a sandstone sample measured by Wang et al. (2015b) and the model prediction using the lognormal PSD with fitting parameters of r_m = 127 μm, s = 0.1, r_{min} = 5 μm and r_{max} = 700 μm.

approximately $\pm 10\%$ that is deduced from Fig. 4 of Wang et al. (2015b). The proposed model with the lognormal PSD is used to reproduce experimental data by taking fitting parameters of r_m = 127 μm, s = 0.1, r_{min} = 5 μm and r_{max} = 700 μm. It is seen that the proposed model using the lognormal PSD can reproduce the main trend of experimental data. For simplicity, we do not show the prediction from the fractal PSD, as it can not match the behavior of measured data. Note that r_m = 127 μm is comparable to the effective pore radius of 358 μm of the sample as reported by Wang et al. (2015b).

Figure 11 shows the variation of $C_{EK}^{rel,*}(\omega)$ as a function of the frequency ω measured by Glover et al. (2012a) for Ottawa sand with modal grain radius of 235 μm saturated by 10^{-3} mol/L NaCl electrolyte as shown by symbols: (a) magnitude, (b) real part, and (c) imaginary part of $C_{EK}^{rel,*}(\omega)$. The proposed model with the lognormal and fractal distributions is used to reproduce the experimental data. For the lognormal distribution, the fitting parameters are r_m = 55 μm, s = 0.1, r_{min} = 1.05 μm and r_{max} = 105 μm. For the fractal distribution, the fitting parameters are D_f = 1.1, r_{min} = 1.05 μm and r_{max} = 105 μm. Note that r_m = 55 μm is quite close to the effective pore radius r_p = 67 μm reported by Glover et al. (2012a) for the Ottawa sand. It is seen that the proposed model with the lognormal PSD provides a very good match with experimental data. However, the proposed model with the fractal PSD is only in good agreement with data at low frequencies. It indicates that the fractal PSD may not be not pertinent for the Ottawa sand, which exhibits a narrow PSD.

Previous works in the literature provide with models for the dynamic streaming potential coupling coefficient in porous media. For example, in its pioneering work, Pride (1994) provided a model for the dynamic streaming potential coupling coefficient in porous media as

$$C_{EK}^{rel,*}(\omega) = \left[1 - i\frac{m^*}{4}\frac{\omega}{\omega_t}\left\{1 - \frac{\lambda_d}{\Lambda}\right\}^2\left\{1 - i^{3/2}\lambda_d\sqrt{\frac{\omega\rho_w}{\eta_w}}\right\}^2\right]^{-1/2} \tag{32}$$

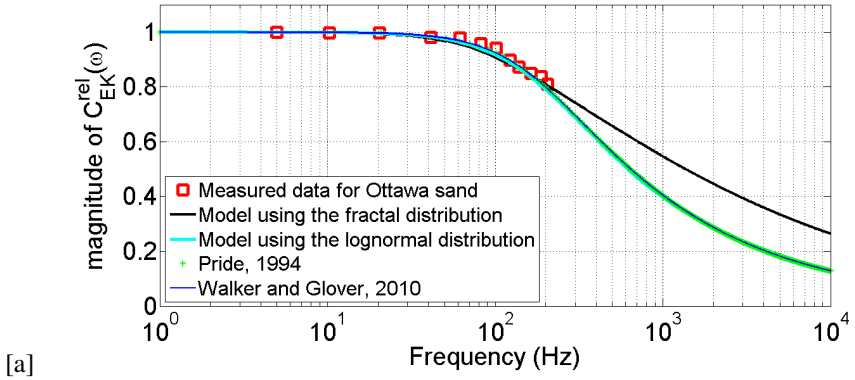

[a]

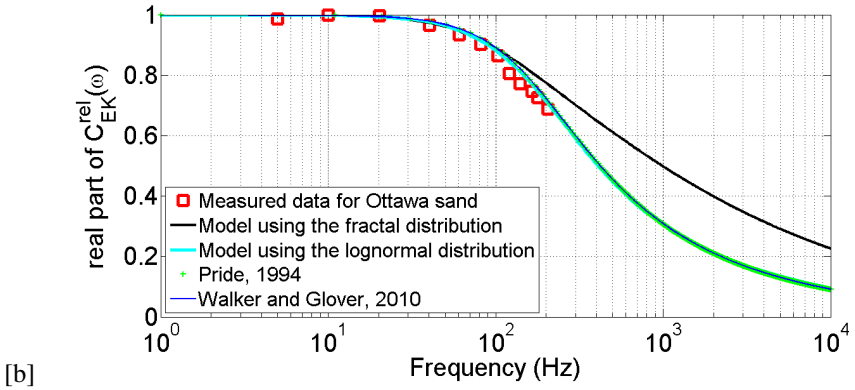

[b]

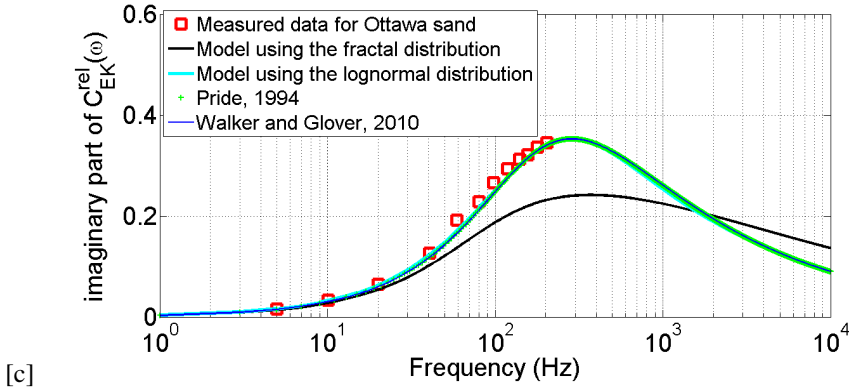

[c]

Figure 11. The dynamic streaming potential coefficient as a function of frequency. Experimental data is obtained from Glover et al. (2012a) for Ottawa sand (ϕ = 0.32, k = 1.19×10^{-10}m^2) and the predictions are from the proposed model, the models by Pride (1994) and Walker & Glover (2010): (a) Magnitude of the $C_{EK}^{rel}(\omega)$, (b) real component $C_{EK}^{rel}(\omega)$, and (c) imaginary component of $C_{EK}^{rel}(\omega)$.

where

$$\omega_t = \frac{\phi \eta_w}{\tau k \rho_w} \tag{33}$$

and

$$m^* = \frac{\phi \Lambda^2}{\tau k}. \tag{34}$$

From Eq. (32) to Eq. (34), λ_d (m) is the Debye length and Λ is the characteristic length scale.

The parameter ω_t (rad/s) is the transition frequency. In most geological media, the condition that λ_d is much smaller than Λ is normally satisfied (Jougnot et al. 2019). Therefore, a significant simplification can be made on Eq. (32) as performed by Walker & Glover (2010):

$$C_{EK}^{rel,*}(\omega) = \left[1 - i\frac{m^*}{4}\frac{\omega}{\omega_t}\right]^{-1/2}. \tag{35}$$

As reported by Glover et al. (2012a) for the Ottawa sand, we have τ = 1.52, ϕ = 0.32, k = 1.19×10^{-10}m^2. The Debye length is calculated to be λ_d = 9.66 nm for 10^{-3} mol/L NaCl electrolyte. The characteristic length scale Λ is found to be 62 μm by fitting. It is seen that the models given by Pride (1994) and Walker & Glover (2010) also provide a very good match with experimental data with the suitable fitting parameter Λ. However, it is important to remark that our proposed approach is designed to allow for virtually any PSD. We only analyze two cases (fractal and lognormal PSDs) in this work. However, our approach permits to compute the response for the double-lognormal PSD, for example, a case that can not be explored using the models given by Pride (1994) or Walker & Glover (2010), which are restricted to only one characteristic length scale Λ.

4 CONCLUSIONS

We have proposed a physically-based model for the frequency dependence of the streaming potential coupling coefficient $C_{EK}(\omega)$ by conceptualizing a porous medium as a bundle of tortuous capillaries and using the lognormal and fractal PSDs. The surface electrical conductivity was also taken into account in the proposed approach. It is seen that $C_{EK}(\omega)$ is a complex function depending on the properties of water (η, σ_w, ϵ), mineral-water interfaces (ζ, Σ_s), microstructural parameters of porous media (D_f, r_{min}, r_{max} for the fractal PSD and r_m, s, r_{min}, r_{max} for the lognormal PSD) and frequency. The results also show that the PSD does not have effect on the quasi-static streaming potential coupling coefficient as reported in the literature when the surface conductivity is negligible. Parameters influencing $C_{EK}(\omega)$ are investigated and explained based on the PSD and the transition angular frequency. The proposed model is then compared with published data and other published models. We found that the proposed model using the lognormal PSD is in very good agreement with the experimental data and previous models in the literature. The proposed model using the fractal PSD provide a good match with published data for sandstone samples but not for the sand samples. The reason may be that the fractal PSD is not pertinent for samples with narrow PSDs. Our results suggest that the PSD of porous media plays an crucial role in the dynamic behaviour of $C_{EK}(\omega)$. Finally, we remark that the proposed approach works for virtually any PSD, including ones that can be directly measured from rock characterization. This particular feature makes this model more versatile than

previous models available in literature. A model for $C_{EK}(\omega)$ under unsaturated conditions using the proposed technique will be performed in our future work.

ACKNOWLEDGMENTS

This research is funded by Vietnam National Foundation for Science and Technology Development (NAFOSTED) under grant number 103.99-2019.316.

Data Availability Statement

The data underlying this article will be shared on reasonable request to the corresponding author.

REFERENCES

Birdi, K. S., 2008. *Handbook of Surface and Colloid Chemistry, Third Edition*, CRC Press.

Butler, K. E., 1996. *Seismoelectric effects of electrokinetic origin*, PhD thesis, University of British Columbia.

Cai, J. & Yu, B., 2010. Prediction of maximum pore size of porous media based on fractal geometry, *Fractals*, **18**, 417–423.

Cherubini, A., Garcia, B., Cerepi, A., & Revil, A., 2018. Streaming potential coupling coefficient and transport properties of unsaturated carbonate rocks, *Vadose Zone Journal*, **17**(1), 180030.

Chu, Z., Zhou, G., & Li, R., 2020. Enhanced fractal capillary bundle model for effective thermal conductivity of composite-porous geomaterials, *International Communications in Heat and Mass Transfer*, **113**, 104527.

Dupuis, J. C., Butler, K. E., Kepic, A. W., & Harris, B. D., 2009. Anatomy of a seismoelectric conversion: Measurements and conceptual modeling in boreholes penetrating a sandy aquifer, *Journal of Geophysical Research: Solid Earth*, **114**(B10).

Frenkel, J., 1944. On the theory of seismic and seismoelectric phenomena in a moist soil, *Journal of Physics (in Russian*, pp. 230–241.

Garambois, S. & Dietrich, M., 2001. Seismoelectric wave conversions in porous media: field measurements and transfer function analysis, *Geophysics*, **66**(2), 1417–1430.

Ghanbarian, B., 2020. Applications of critical path analysis to uniform grain packings with narrow conductance distributions: Ii. water relative permeability, *Advances in Water Resources*, **137**, 103524.

Glover, P., Walker, E., Ruel, J., & Tardif, E., 2012a. Frequency-dependent streaming potential of porous media-part 2: Experimental measurement of unconsolidated materials, *International Journal of Geophysics*, **2012**.

Glover, P. W. J. & Dery, N., 2010. Streaming potential coupling coefficient of quartz glass bead packs: Dependence on grain diameter, pore size, and pore throat radius, *Geophysics*, **75**(6), F225–F241.

Glover, P. W. J., Walker, E., & Jackson, M., 2012b. Streaming-potential coefficient of reservoir rock: A theoretical model, *Geophysics*, **77(2)**(2), D17–D43.

Guarracino, L. & Jougnot, D., 2018. A physically based analytical model to describe effective excess charge for streaming potential generation in water saturated porous media, *Journal of Geophysical Research: Solid Earth*, **123**(1), 52–65.

Hu, H., Guan, W., & Harris, J. M., 2007. Theoretical simulation of electroacoustic borehole logging in a fluid-saturated porous formation, *The Journal of the Acoustical Society of America*, **122**(1), 135–145.

Jaafar, M. Z., Vinogradov, J., & Jackson, M. D., 2009. Measurement of streaming potential coupling coefficient in sandstones saturated with high salinity nacl brine, *Geophysical Research Letters*, **36**(L21306), doi:10.1029/2009GL040549.

Jackson, M. & Leinov, E., 2012. On the validity of the thin and thick double-layer assumptions when calculating streaming currents in porous media, *International Journal of Geophysics*, **2012**.

Jackson, M., Butler, A., & Vinogradov, J., 2012. Measurements of spontaneous potential in chalk with application to aquifer characterization in the southern uk, *Quarterly Journal of Engineering Geology Hydrogeology*, **45**(4), 457–471.

Jackson, M. D., 2010. Multiphase electrokinetic coupling: Insights into the impact of fluid and charge distribution at the pore scale from a bundle of capillary tubes model, *Journal of Geophysical Research: Solid Earth*, **115**(B7).

Jardani, A., Revil, A., Boleve, A., Crespy, A., Dupont, J.-P., Barrash, W., & Malama, B., 2007. Tomography of the darcy velocity from self-potential measurements, *Geophysical Research Letters*, **34**(24).

Jougnot, D. & Solazzi, S. G., 2021. Predicting the frequency-dependent effective excess charge density: A new up-scaling approach for seismoelectric modelling, *Geophysics*, **86**(3), 1–10.

Jougnot, D., Linde, N., Revil, A., & Doussan, C., 2012. Derivation of soil-specific streaming potential electrical parameters from hydrodynamic characteristics of partially saturated soils, *Vadose Zone Journal*, **11**(1), 272–286.

Jougnot, D., Rubino, J. G., Carbajal, M. R., Linde, N., & Holliger, K., 2013. Seismoelectric effects due to mesoscopic heterogeneities, *Geophysical Research Letters*, **40**(10), 2033–2037.

Jougnot, D., Mendieta, A., Leroy, P., & Maineult, A., 2019. Exploring the effect of the pore size distribution on the streaming potential generation in saturated porous media, insight from pore network simulations, *Journal of Geophysical Research: Solid Earth*, **124**(6), 5315–5335.

Jougnot, D., Roubinet, D., Guarracino, L., & Maineult, A., 2020. *Modeling Streaming Potential in Porous and Fractured Media, Description and Benefits of the Effective Excess Charge Density Approach*, In: Biswas A., Sharma S. (eds) Advances in Modeling and Interpretation in Near Surface Geophysics. Springer Geophysics. Springer, Cham.

Jouniaux, L. & Ishido, T., 2012. Electrokinetics in earth sciences: A tutorial, *International Journal of Geophysics*, **2012, Article ID 286107**, 16 pages, doi:10.1155/2012/286107.

Jouniaux, L. & Zyserman, F., 2016. A review on electrokinetically induced seismo-electrics, electro-seismics, and seismo-magnetics for earth sciences, *Solid Earth*, **7**(1), 249–284.

Kormiltsev, V. V., Ratushnyak, A. N., & Shapiro, V. A., 1998. Three-dimensional modeling of electric and

magnetic fields induced by the fluid flow movement in porous media, *Physics of the Earth and Planetary Interiors*, **105**(3), 109 – 118.

Kosugi, K., 1994. Three-parameter lognormal distribution model for soil water retention, *Water Resources Research*, **30**(4), 891–901.

Mikhailov, O. V., Queen, J., & Toksz, M. N., 2000. Using borehole electroseismic measurements to detect and characterize fractured (permeable) zones, *GEOPHYSICS*, **65**(4), 1098–1112.

Morgan, F. D., Williams, E. R., & Madden, T. R., 1989. Streaming potential properties of westerly granite with applications, *Journal of Geophysical Research*, **94**(B9), 12.449–12.461.

Nghia A, N. V., Jougnot, D., Thanh, L. D., Van Do, P., Thuy, T. T. C., Hue, D. T., & Hung, N. M., 2021. Predicting water flow in fully and partially saturated porous media: a new fractal-based permeability model, *Hydrogeology Journal*, **29**, 20172031.

Niu, Q., Fratta, D., & Wang, Y.-H., 2015. The use of electrical conductivity measurements in the prediction of hydraulic conductivity of unsaturated soils, *Journal of Hydrology*, **522**, 475 – 487.

Packard, R. G., 1953. Streaming potentials across glass capillaries for sinusoidal pressure, *The Journal of Chemical Physics*, **21**(2), 303–307.

Peng, R., Di, B., Glover, P. W. J., Wei, J., Lorinczi, P., Liu, Z., & Li, H., 2020. Seismo-electric conversion in shale: experiment and analytical modelling, *Geophysical Journal International*, **223**(2), 725–745.

Pride, S., 1994. Governing equations for the coupled electromagnetics and acoustics of porous media, *Physical Review B*, **50**(21), 15678–15696.

Pride, S. R. & Garambois, S., 2005. Electroseismic wave theory of frenkel and more recent developments, *Journal of Engineering Mechanics*, **131**(9), 898–907.

Pride, S. R. & Morgan, F. D., 1991. Electrokinetic dissipation induced by seismic waves, *Geophysics*, **56**(7), 914–925.

Rembert, F., Jougnot, D., & Guarracino, L., 2020. A fractal model for the electrical conductivity of water-saturated porous media during mineral precipitation-dissolution processes, *Advances in Water Resources*, **145**, 103742.

Reppert, P. M., Morgan, F. D., Lesmes, D. P., & Jouniaux, L., 2001. Frequency-dependent streaming potentials, *Journal of Colloid and Interface Science*, **234**(1), 194 – 203.

Revil, A. & Glover, P. W. J., 1998. Nature of surface electrical conductivity in natural sands, sandstones, and clays, *Geophysical Research Letters*, **25**(5), 691–694.

Revil, A. & Jardani, A., 2010. Stochastic inversion of permeability and dispersivities from time lapse self-potential measurements: A controlled sandbox study, *Geophysical Research Letters*, **37**(11).

Revil, A. & Jardani, A., 2013. *The Self-Potential Method: Theory and Applications in Environmental Geosciences*, Cambridge University Press.

Revil, A. & Leroy, P., 2004. Constitutive equations for ionic transport in porous shales, *Journal of Geophysical Research: Solid Earth*, **109**(B3), B03208.

Revil, A. & Mahardika, H., 2013. Coupled hydromechanical and electromagnetic disturbances in unsaturated

porous materials, *Water Resources Research*, **49**, 744–766.

Revil, A., Pezard, P. A., & Glover, P. W. J., 1999. Streaming potential in porous media 1. theory of the zeta potential, *Journal of Geophysical Research*, **104**(B9), 20021–20031.

Revil, A., Linde, N., Cerepi, A., Jougnot, D., Matthi, S., & Finsterle, S., 2007. Electrokinetic coupling in unsaturated porous media, *Journal of Colloid and Interface Science*, **313**(1), 315 – 327.

Revil, A., Jardani, A., Sava, P., & Haas, A., 2015. *The Seismoelectric Method: Theory and Applications*, John Wiley and Sons.

Rice, C. & Whitehead, R., 1965. Electrokinetic flow in a narrow cylindrical capillary, *J. Phys. Chem.*, **69**(11), 4017–4024.

Shi, P., Guan, W., & Hu, H., 2018. Dependence of dynamic electrokinetic-coupling-coefficient on the electric double layer thickness of fluid-filled porous formations, *Annals of Geophysics*, **61**(3), SE340.

Smoluchowski, M., 1903. Contribution à la theorie de l'endosmose electrique et de quelques phenomènes correlatifs, *Bulletin international de l'Academie des Sciences de Cracovie*, **8**, 182 – 200.

Solazzi, S. G., Rubino, J. G., Jougnot, D., & Holliger, K., 2020. Dynamic permeability functions for partially saturated porous media, *Geophysical Journal International*, **221**(2), 1182–1189.

Soldi, M., Guarracino, L., & Jougnot, D., 2019. An analytical effective excess charge density model to predict the streaming potential generated by unsaturated flow, *Geophysical Journal International*, **216**(1), 380–394.

Tardif, E., Glover, P. W. J., & Ruel, J., 2011. Frequency-dependent streaming potential of ottawa sand, *Journal of Geophysical Research: Solid Earth*, **116**(B4), n/a–n/a.

Thanh, L., Jougnot, D., Do, P., Ca, N., & Hien, N., 2020a. A physically based model for the streaming potential coupling coefficient in partially saturated porous media, *Water*, **12**(5), 1588.

Thanh, L. D., Van Do, P., Van Nghia, N., & Ca, N. X., 2018. A fractal model for streaming potential coefficient in porous media, *Geophysical Prospecting*, **66**(4), 753–766.

Thanh, L. D., Jougnot, D., Van Do, P., & Van Nghia A, N., 2019. A physically based model for the electrical conductivity of water-saturated porous media, *Geophysical Journal International*, **219**(2), 866–876.

Thanh, L. D., Jougnot, D., Van Do, P., A, N. V. N., Tuyen, V. P., Ca, N. X., & Hien, N. T., 2020b. A physically based model for the electrical conductivity of partially saturated porous media, *Geophysical Journal International*, **223**(2), 993–1006.

Thanh, L. D., Jougnot, D., Van Do, P., Mendieta, A., Ca, N. X., Hoa, V. X., Tan, P. M., & Hien, N. T., 2020c. Electroosmotic coupling in porous media, a new model based on a fractal upscaling procedure, *Transport in Porous Media*, **134**, 249274.

Thompson, A. H., Sumner, J. R., & Hornbostel, S. C., 2007. Electromagnetic-to-seismic conversion: a new direct hydrocarbon indicator, *The leading Edge*, **26**(4), 428–435.

Thompson, R. R., 1939. A note on the seismic-electric phenomenon, *Geophysics*, **4**(2), 102–105.

Tyler, S. W. & Wheatcraft, S. W., 1990. Fractal processes in soil water retention, *Water Resources Research*, **26**(5), 1047–1054.

Vinogradov, J., Hill, R., & Jougnot, D., 2021. Influence of pore size distribution on the electrokinetic coupling

coefficient in two-phase flow conditions, *Water*, **13**(17).

Walker, E. & Glover, P. W. J., 2010. Permeability models of porous media: Characteristic length scales, scaling constants and time-dependent electrokinetic coupling, *GEOPHYSICS*, **75**(6), E235–E246.

Wang, J., Hu, H., & Guan, W., 2015a. Experimental measurements of seismoelectric signals in borehole models, *Geophysical Journal International*, **203**(3), 1937–1945.

Wang, J., Hu, H., Guan, W., & Li, H., 2015b. Electrokinetic experimental study on saturated rock samples: zeta potential and surface conductance, *Geophysical Journal International*, **201**(2), 869–877.

Wang, J., Hu, H., & Guan, W., 2016. The evaluation of rock permeability with streaming current measurements, *Geophysical Journal International*, **206**(3), 1563–1573.

Watanabe, K. & Flury, M., 2008. Capillary bundle model of hydraulic conductivity for frozen soil, *Water Resources Research*, **44**(12).

Yu, B. & Cheng, P., 2002. A fractal permeability model for bi-dispersed porous media, *International Journal of Heat and Mass Transfer*, **45**(14), 2983–2993.

Zhou, M.-Y. & Sheng, P., 1989. First-principles calculations of dynamic permeability in porous media, *Physical Review B*, **39**, 12027–12039.

Zhu, Z. & Toksoz, M. N., 2013. Experimental measurements of the streaming potential and seismoelectric conversion in berea sandstone, *Geophysical Prospecting*, **61**, 688–700.

Zhu, Z., Haartsen, M. W., & Toksz, M. N., 1999. Experimental studies of electrokinetic conversions in fluid-saturated borehole models, *GEOPHYSICS*, **64**(5), 1349–1356.